Bubble migration and the transition from bubble to plug flow in vertical channels

Proceedings of The 2nd International Conference on
Multiphase Flow '95-Kyoto
April 3-7, 1995
Kyoto, Japan

Bubble Migration and Transition to Plug Flow in Vertical Channels

C. W. M. van der Geld and B. A. Brand

Eindhoven University of Technology, Faculty of Mechanical Engineering
Room WH 3.144, P.O. box 513, 5600 MB Eindhoven, THE NETHERLANDS
Fax: +31-40-44-17-49
E-mail: cwm@wop.wtb.tue.nl or bob@wop.wtb.tue.nl

ABSTRACT

Void fraction profiles in upflow (five different cross-sections) and downflow (rectangular cross-section) have been measured and interpreted with the aid of the migration dependencies. The dependencies of the bubble-to-plug flow pattern transition on void fractions, tube diameter and temperature have been measured. If the bubble diameter, D_b, exceeds 1 mm, the bubble moves to the wall if $D_b < 6$ mm and if flow is upward. In downflow, the opposite behaviour is found. In a rectangular cross-section, these bubbles preferably migrate towards the largest side in upflow because of secondary flows.

INTRODUCTION

The transition from bubble- to plugflow can be recognized from the void fraction profiles (PDFs). These profiles show a high concentration of void in the centre of the channel (approximately 0.20). The exact value of this concentration are not important here since that value is related to instabilities that develop in the flow direction in the channel (Lammers [1]). High concentrations of void (upto 50%) have been recorded without there being any transition to plugflow. Because of the difference between bubble- and plugflow, different surface-energies, the conditions for the coalescence of bubbles need to be favourable (Chesters [2]). These conditions are governed by hydrodynamical and physicochemical factors, both of which are not the subject of this paper. Here, it is tried to create one single condition in five channels of varying cross-section and at several average void fractions. The question is addressed whether the void fraction in the centre of the channel is more important than the average void fraction under conditions that usually prevail in the laboratory. At the same time, the influence of channel diameter on the bubble-to-plug transition will be considered.

Over the years many experiments of this kind were performed by others. Most of these were performed in circular channels with small diameters. Void profiles were explained by considering the migratory behaviour of individual bubbles. See e.g. Žun, Serizawa, Sekoguchi and others [3-5]. Downflow was studied by e.g. Oshinowo & Charles [6]. The motion of individual bubbles and the possible mechanisms were studied by e.g. Žun [7] and Aybers & Tapucu [8,9]. Forces on a bubble were studied by e.g. Leal [10] and Auton [11].

In this paper, the equivalent diameter is determined at which the larger bubbles do not go to the wall but stay in the centre. Also the influence of the shape of the channel (circular or rectangular) on migration and void fraction profiles is examined. Tube diameters up to 90 mm have been employed. Again, these result are related to the transition to plug flow.

1. EXPERIMENTAL

1.1 Test rigs

Two test-rigs have been used in the experiments. (See table 1.) The first one consists of four vertical, circular, perspex channels of different diameter. These channels are being fed from *one* storage tank so that the water quality, ambient pressure and temperature are the same for all channels. Superficial water and air velocity are controlled separately for each channel. Each channel has a length of at least 75 equivalent diameters. In it present form, it can only be used for upflow experiments.

The other test-rig consists of a single vertical rectangular channel. It is constructed in a modular way. Most

Table 1
The test rigs used

Loop	Dimensions CS	H	L1	L2	Flow	Exp
4-Channel	26 mm Ø	4.0	3.0		U	VT
	40 mm Ø	5.0	3.8	3.0	U	VTM
	60 mm Ø	5.9	4.5	2.9	U	VTM
	90 mm Ø	7.7	6.0	4.4	U	VTM
Rectangular	100 x 35 mm^2	3.0	2.8	2.4	U/D	VTM

CS: cross-section, H: total height [m], L1: Distance between bubbly flow air inlet and local void probe [m], L2: Distance between single bubble injector and optical observation point [m], Exp: Experiments performed, U: Upflow, D: Downflow, V: Void measurements, T: Transition from bubble to plugflow, M: Migration experiments.

sections (or modules) are "blind" stainless steel sections, but the relevant sections have glass walls along the long walls. This test-rig can be configured for both up- and downflow experiments.

Both rigs are loops, open to the atmosphere.

The water used in all experiments is a mixture of 50% tap water and 50% demineralized water. The air comes from a central air supply net and is filtered using an oil-catcher and a 5 μm filter.

1.2 Bubble generators

To create a "flow" of single *individual* bubbles, each bubble at least 10 bubble diameters apart from the next one, bubble injectors of different size and material have been employed: ranging from glass capillaries with an orifice of 20 μm at the end to brass capillaries with an orifice of 10 mm in the side-wall. A needle-valve is mounted just in front of the injector to allow accurate control over the amount of air injected and thus over the bubble size. The injectors can be moved so that bubbles are injected in the centre of the channel or near the wall. These injectors have been used for the migration experiments in all channels. In the rectangular section, bubbles have been injected in the centre and near the shorter wall of the rectangle.

For void-distribution measurements, other injectors have been employed. In the 4-channel loop, bubbly flow is created using an air-inlet of sintered glass, flush mounted in the wall in each channel. In the rectangular section, the air inlet consists of four panels of sintered bronze, also flush mounted in the wall.

1.3 Bubble size and migration measurements

In the migration experiments it is essential to determine the position of each individual bubble in the channel. In both test-rigs, this is done by using a set of mirrors (see figures 1 and 2). The result is recorded using photography, video and high-speed cine-film. Shutter times of 1/1000th of a second are used with the still-photo and video-camera. Upto 1000 frames/second are

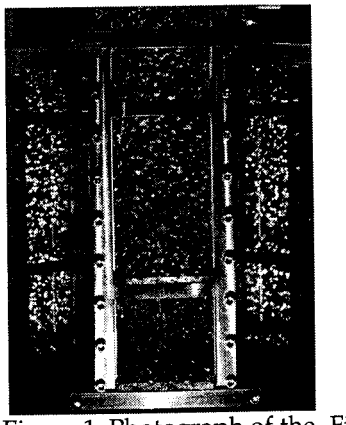

Figure 1: Photograph of the rectangular section with mirrors

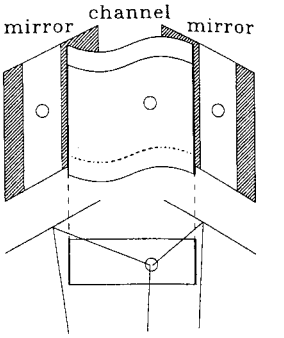

Figure 2: Rectangular section: Bubble position determination

used with the high-speed cine-film camera. The channels are illuminated using a 1000 W incandescent lamp with reflector and diffuser.

The position of a bubble is calculated from the frontal view and the images in the mirrors. The refractive index of the water and the perspex and the curvature of both inner and outer channel wall (for the circular channels) is taken into account. The position of the bubbles is determined with an accuracy better than 3%. The bubble size is also determined using these images.

The position of the same bubble is determined in several consecutive frames of the video- or high-speed cinefilm. That way, the path of the bubble is traced out, both in stagnant water and in flow.

1.4 Void fraction measurements

Local void fractions have been measured using so called Local Void Probes (LVPs).

Two different types have been used: In the circular channels, conductivity probes have been used. These probes have their tip bent upstream to prevent bubbles from either being deflected by the flow around the probe (and thus never be measured) or from becoming entangled in the wake behind the probe (and thus disturbing the measurement too much). The probes are calibrated using a separate calibration rig with quick closing valves (see e.g. Hetsroni [12]). To correctly interpret the results, software is developed with two trigger levels. These levels allow the easy discrimination of consecutive bubbles. The observation point is at least 65 equivalent diameters downstream of the bubble generator. The probes can be traversed along the radius of the channel.

In the rectangular channel, an optical LVP is used. Again, it has its tip bent upstream for the same reasons as stated above. A special feature of this probe is that, after calibration, it gives the rise-velocity of a bubble as well. Since the flow pattern in a rectangular channel is not rotational symmetrical, a special mounting has been developed which allows for the scanning of an entire quarter section of the cross-section.

To verify the void profiles in both test-rigs, an Overall

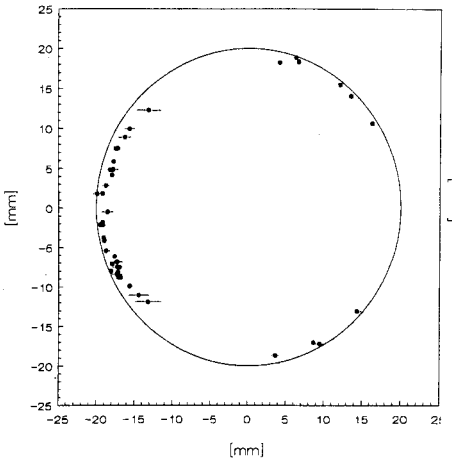

Figure 3: Wall-distribution. D_{tube} = 40 mm, $v_{s,l}$ = 0.20 m/s, $D_{eq,b}$ = 2 mm.

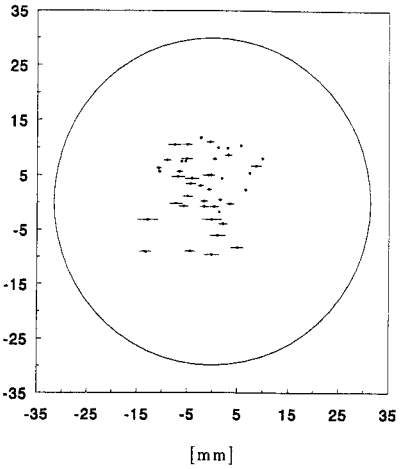

Figure 4: Central-distribution. D_{tube} = 60 mm, $v_{s,l}$ = 0.25 m/s, $D_{eq,b}$ = 0.9 mm

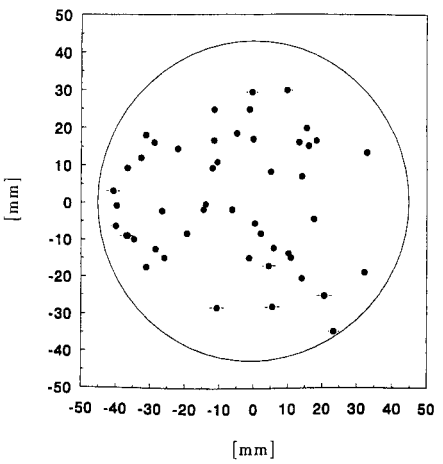

Figure 5: Spread-out distribution. D_{tube} = 90 mm, $v_{s,l}$ = 0.0 m/s, $D_{eq,b}$ = 6 mm.

Void Meter (OVM) is being used. This sensor measures the overall-mixture conductivity over the channel's cross-section and compares it to a reference OVM in the feeding pipe that is always immersed in 100% water (Van der Geld & Van Koppen [13]).

2 RESULTS

In this section, the measurements results are being presented that will be analyzed an discussed in section 3.

2.1 Migration experiments

Bubbles, at least 10 equivalent diameters, $D_{eq,b}$, separated, have been generated in the centre of the channel with an equivalent diameter ranging from 0.8 to 15 mm. The position has been determined for a large number of bubbles at 30 cm and 65 channel diameters downstream of the injection point. In some experiments, bubbles have also been injected near the wall. Water velocities range from stagnant to 90 cm/s. The results are summarized in table 2.

In figures 3 to 5, each mark represents an individual bubble passage. The closer the marks, the higher the chance to find a bubble in the area occupied by the marks. To quantify the notions of "near the wall" and "in the centre" the ratio of this area to the channel cross-sectional area is also given in table 2. The lower the number, the more the bubbles move in one specific region. A distribution is said to be spread out when the marks cover a disc with radius of at least half the channel. In this case, the area-ratio has a value of 0.5 or more. Usually "spread" means that the bubbles do not tend to the wall. An example is given in figure 5.

The path of individual bubbles is determined. Three types of bubble path are distinguished for stagnant water and for flow.

I Bubbles that move virtually undisturbed upwards. These bubbles have a diameter of around 1 mm or less.

II Bubbles that display a helical-path or zig-zag motion with an amplitude that exceeds $D_{eq,b}$ by at least a factor 2. These bubbles have an equivalent diameter of around 2 mm. See figure 6.

III Bubbles that display a rocking or wobbling motion with an amplitude in the order of $D_{eq,b}$. All bubbles with $D_{eq,b}$ > 2 mm exhibit this motion. These bubbles deform into asymmetric shapes. See figure 9.

See figure 7 for both the side-view and the view from above of a typical bubble path as recorded by high-speed cine-film with $v_{s,l}$ = 0.25 m/s in the 90 mm channel (1000 frames/s, 20 frames between consecutive marks). In the circular tubes, no helical motion has been measured if the bubble was moving close to the wall. In that case, the bubble path was zig-zag in a plane tangent to the tube wall. See figures 6 and 7.

2.2 Void fraction distribution experiments

Bubbly flow has been generated using sintered materials as described in section 1.2. Again, the water velocity ranged from stagnant to 90 cm/s. The superficial air velocity has been raised up to the point where spherical cap bubbles became visible in the flow. Typical void profiles are given in figure 8 for circular channels and figure 10 (upflow) and figure 11 (downflow) for the rectangular channel.

Reversal of the flow direction reverses the migratory behaviour and the void distribution. Our experiments with downflow show that:

- Bubbles do not move to the wall.
- The bubble categories listed above apply equally well for downflow.

2.3 Bubble-to-plug transition experiments

The experiments show that for an increasing channel diameter, the transition from bubble- to plugflow occurs at higher superficial gas velocities. For increasing temperature, the transition occurs at lower superficial gas velocities. The temperature has been increased from 21°C (ambient temperature) to 40°C and 60°C.

The average void fraction, approximately 20%, at the

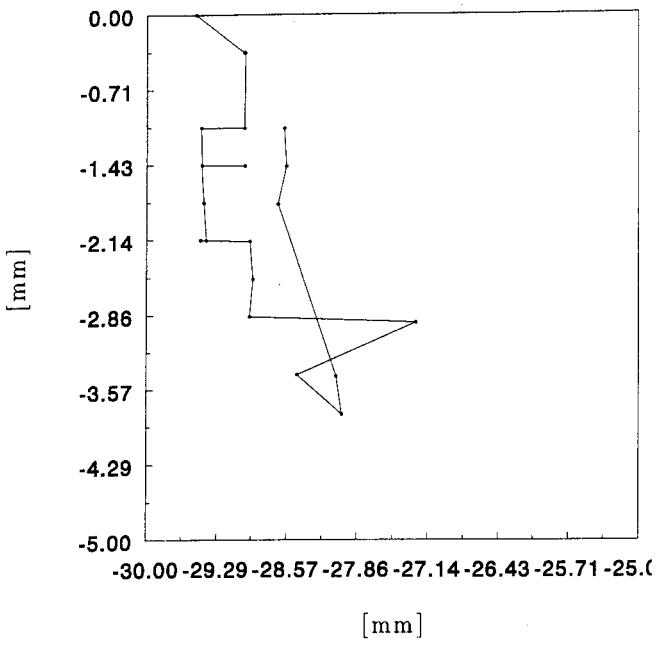

Figure 6: Path of a type II bubble. D_{tube} = 60 mm, $v_{s,l}$ = 0.25 m/s, $D_{eq,b}$ = 2 mm.

transition is independent of the channel diameter and weakly affected by the superficial water velocity. The void profile becomes parabolic near the point of bubble-plug transition. I.e., no wall-peaking occurs.

In downflow, the void profile observed near the point of bubble-plug transition is parabolic, as it is in upflow.

3 ANALYSIS AND CONCLUSIONS

3.1 Bubble migration

Only the smallest bubbles, $D_{eq,b}$ < 1 mm, do not show helical or zig-zag motion. Larger ones all have a wobbling or rocking motion, even if water is flowing. It has been shown (see e.g. Duineveld [14]) that this zig-zag or wobble path is intimately connected to the shedding of vortices downstream of the bubble.

Turbulent diffusion causes a stochastic spread of bubbles over the channel diameter around the injection point. This explains the increasing spreading for 0.8 mm bubbles in the 60 mm channel with increasing $v_{s,l}$. See table 2 and the appendix.

Bubbles that do move towards the channel wall probably do so because of the Auton/Žun [7,11] liftforce.

$$\vec{F}_{lift} = \rho_f \frac{1}{6} \pi D_{eq,b}^3 \vec{\omega} \times (\vec{u}_b - \vec{u}_f)$$

where ρ_f denotes the fluid mass density, $D_{eq,b}$ the equivalent bubble diameter, $\vec{\omega}$ the vorticity, $\vec{u}_b$ the velocity of the bubble and $\vec{u}_f$ the velocity of the fluid. This expression for the liftforce was derived [11] for small velocity gradients and small bubble sizes under the assumption that: $|\omega D_b / U_{rel}| \ll 1$, where ω is the vorticity and U_{rel} the relative velocity.

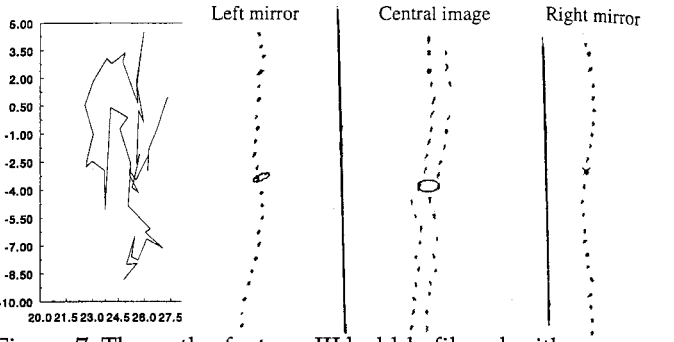

Figure 7: The path of a type III bubble filmed with high-speed camera. D_{tube} = 90 mm, $v_{s,l}$ = 0.25 m/s, $D_{eq,b}$ = 10 mm. Left: dimensions in mm, right: distance between lines in reality 90 mm.

Note that $\vec{F}_{lift}$ changes sign when the liquid flow is reversed, which explains the opposite migration trends in up- and downflow.

The maximum diameter of bubbles that still move towards the wall, around 6 mm, exceeds the diameter found by other people for smaller bore channels. E.g. Sekaguchi (Žun [4]) found wall-peaking in a 17,7 mm Ø channel with $v_{s,l}$ = 2 m/s for bubbles with $D_{eq,b}$ = 3.0 and 4.0 mm, but core-peaking for $D_{eq,b}$ = 5.0 mm. Žun [4] found wall-peaking in a 12,7 mm square channel with $v_{s,l}$ =0.44 m/s for bubbles with $D_{eq,b}$ = 4.7 mm, but core peaking for $D_{eq,b}$ = 5.1 mm.

Bubble motion for diameters larger than 1 mm is hardly affected by the presence of surfactants (Duineveld [14]). So for those bubbles of concern, physicochemical influences cannot explain the difference of our migration measurement with those of Sekaguchi and Žun. It might be that the bubble diameter for which the migration towards the tube wall stops depends on the tube diameter, although this does not follow from our present set of data.

If bubble diameters exceeds 6 mm, the bubbles spread out and do not move to the wall any more. Our measurement clearly show that in this case migration is as if the liftforce was absent. There is no need to invoke a force that drives bubbles to the core. There is a need, however, to explain what keeps these large bubbles from migrating to the wall. Especially so, since these large bubbles still follow a helical or zig-zag path and since $\vec{F}_{lift}$ is proportional to $D_{eq,b}^3$.

Turbulent diffusion, see the appendix, does not have a directional preference and can hardly be a counteracting agency As for the effect of turbulence bursts, experiments by Yung et al. [15] show that only larger particles may be expelled from the wall by bursts originating at the wall. This effect has not yet been quantified for bubbles , as far as the authors know. However, the authors feel that it is more appropriate not to look for a compensating mechanism but to search for a physical mechanism that makes the lift force inactive. Two suggestions will be given below in section 4.

Bubble migration in the rectangular channel is characterized by a tendency in upflow for bubbles to stay away from the short wall. This striking difference with migratory behaviour in circular channels has not been

reported in the literature so far. This trend is understood by the secondary flows that appear in rectangular channels and in helical tubes (Vlaicu et al [16]).

Secondary flows cause a so called pressure gradient force (see Meng & Van der Geld [17]) acting in lateral direction. For a circular tube, Wang et al [18] used the two-fluid model to derive the following expression for this force:

$$\vec{F}_{pg} = \rho_f (1-\varepsilon_{av}) \frac{1}{6} \pi D_b^3 \left\{ \frac{\partial \overline{(u'_f)^2}}{\partial r} + \frac{\overline{(u'_f)^2} - \overline{(w'_f)^2}}{r} \right\}$$

Here, u'_f and w'_f denote the (undisturbed) liquid velocity fluctuating components in radial and circumferential direction. A similar expression holds in a rectangular channel and can be used to quantify the effect of secondary flow if experimental values for the resulting velocities u' and w' are employed.

3.2 Void fraction determination

As migration measurements show, core-peaking is caused by larger bubbles that diffuse mostly in the centre and the wall peaking is caused by smaller bubbles, $D_{eq,b} < 6$ mm, that move towards the wall.

The construction of the air-inlets is such that at different superficial air- and water velocities bubbles of different $D_{eq,b}$ will be produced. So different bubble-size PDFs occur in different flow conditions, which largely explains the different void profiles as those shown in figure 9. If one eliminates bubble-bubble interaction by releasing a very low quality flow of individual bubbles then one gets two peaks, each of which corresponds to a different bubble diameter (Žun [5]).

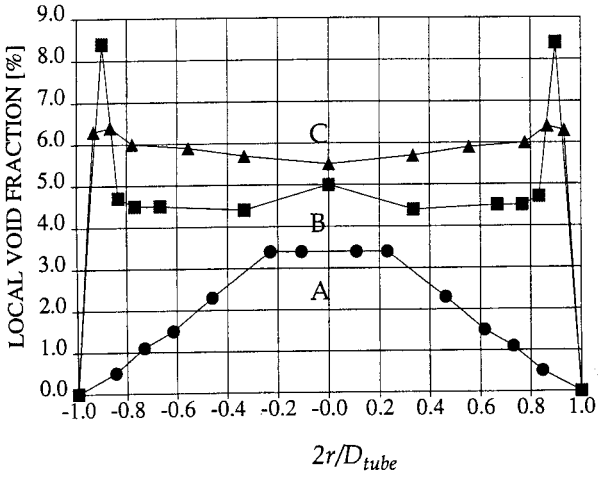

Figure 8: Void profiles in circular channels
A: core-peaking, $D_{tube} = 26$ mm, $v_{sl} = 0.15$ m/s, $D_{eq,b} = 5.5 \pm 1$mm.
B: wall-peaking., $D_{tube} = 60$ mm, $v_{s,l} = 0.50$ m/s, $D_{eq,b} = 4 \pm 1.5$ mm
C: flat with some wall-peaking, $D_{tube} = 90$ mm, $v_{s,l} = 0.26$ m/s, $D_{eq,b} = 5 \pm 1$ mm.

Core peaking can be explained by assuming a great production rate of large bubbles. However, it might well be that also bubble-bubble interactions is involved in the core peaking of flows with relatively high mean void fraction ($\varepsilon_{av} \sim 3 - 30\%$) that we study. See also the numerical work by Žun et al. [7].

Wall-peaking increases with increasing superficial water velocity by constant central void fraction. This is due to the increase in gradient $dv_{sup,l}/dr$ and due to the occurrence of more smaller bubbles as explained above. This effect is independent of the channel diameter and independent of the mean bubble size (decreased from approx 5.5 mm to approximately 1.5 mm by adding a very small volume percentage of ethanol to the water during a particular set of experiments).

The position of the maximum void peak, ε_{max} is independent of the channel diameter but is clearly dependent of the bubble size. Under all flow regimes, ε_{max} lies approximately at distance $D_{eq,b}$ from the wall. With constant superficial water velocity and constant average void fraction, the ratio $\varepsilon_{max}/\varepsilon_c$ is also independent of the channel diameter. Here, ε_c denotes the local void fraction in the centre of the tube.

3.3 Bubble to plug transitions

Coalesce of bubbles not only takes place in the bubbly mixture as a result of density waves (Lammers [1]) and favourable coalescence conditions (Chesters [2]) but also at the injection point. The fact that with increasing superficial gas velocity the wall peaking disappears may imply that, on average, larger bubbles are formed at the inlet and that the bubble-bubble interaction becomes important. If due to the dense packing of bubbles their relative velocity is reduced, flow conditions are such that they favour coalescence (Chesters [2]). In larger bore tubes, the core region that is occupied by larger bubbles is larger than in smaller bore tubes, see also figure 9. The parabolic void fraction profile, characteristic for the transition from bubble to plugflow is therefore more flattened for larger tube diameters. This, and the fact that ε_{av} is independent of D_{tube} at bubble-plug transition, implies that ε_c decreases for increasing D_{tube} at bubble-plug transition, as also follows directly from our measurements. This is attributed to bubble-bubble interactions being such that in larger bore tubes the relative bubble velocity is less and coalescence is fostered.

4 SOME CONCLUDING REMARKS

The preferred location of bubbles with $D_{eq,b} < 6$ mm in the rectangular section, near the larger wall, is a striking phenomenon that shows the importance of secondary flows. The fact that in downflow these bubbles stay away from the wall is important since it demonstrates the applicability of a lift force proportional to

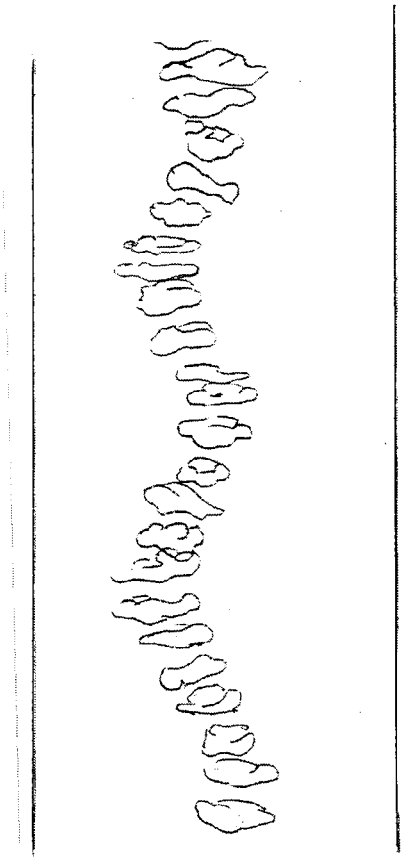

Figure 9: Deformation of type III bubble. Vertical lines are the channel wall, in reality 90 mm apart. $v_{s,l} = 0$.

$\vec{\omega} \times (\vec{u}_b - \vec{u}_f)$. However, the fact that bubbles with $D_{eq,b} >$ 6 mm do not go to the wall rather than go to the channel centre is a conclusion that deserves further elaboration. Two hypotheses have come up to explain this tendency to inactivate the lift force:

- These bubbles have an asymmetrical shape that may induce an asymmetrical flow field on its own right that in combination with the velocity gradient in the liquid flow field may generate a force on the bubble that compensates the usual action of the aforementioned lift force.
  The gradient is much less in the centre of the channel so the effect is much less there. The asymmetrical deformation may affect the lift force if the bubble experiences a velocity gradient near the wall in such a way that the net lift force is zero near the wall. So on average, large bubbles are kept away from the wall.
- Measurements in the rectangular channel show the effect from secondary flow. It might be that larger bubbles create secondary flows in their wake that are persistent in the channel affecting trailing bubbles. The main flaw in this reasoning is the persistency of these secondary flow: They need to be more persistent than at least 10 equivalent bubble diameters in a flowing medium.

NOMENCLATURE

D_b	Bubble diameter
$D_{eq,b}$	Equivalent bubble diameter
D_{tube}	Tube/channel diameter
Δt	Time of flight
ε_{av}	Average void fraction over cross-sectional area
ε_c	Central void fraction
ε_{max}	Maximum void fraction in a channel
L_b	Bubble lateral displacement
L_e	Characteristic eddy length
$\vec{F}_{lift}$	Liftforce
$\vec{F}_{lift}$	Pressure gradient force
r	Radial distance in channel
ρ_f	Mass-density of fluid
$\vec{u}_b$	Bubble velocity
$\vec{u}_f$	Fluid velocity
u'_f	Radial liquid velocity fluctuation
$v_{s,l}$	Superficial water velocity
w'_f	Circumferential liquid velocity fluctuation
$\vec{\omega}, \omega$	Vorticity

REFERENCES

1. J.H. Lammers, *The Stability of Bubbly Flows*, Ph.D. Thesis, Univ. of Technology, Twente, 1994.
2. A.K. Chesters, *The Modelling of Coalescence Processes in Fluid-Liquid Dispersions: A Review of Current Understandings*, Chem. Eng. Res. Design, July 1991.
3. I. Žun, *The Role of Void-Peaking in Vertical Two-Phase Bubbly Flow*, Conference paper, 2nd int. conf. on multi-phaseflow, London, june 1985.
4. I. Žun, *The Mechanisms of Bubble Non-Homogeneous Distribution in Two-Phase Shear Flow*, Nucl. Eng. & Design. 118 (1990), 155-162.
5. A. Serizawa, I. Kataoka, I. Žun & H. Michiyoshi, *Bubble Size Effects on Phase Distributions*, Conference paper, Japan-US seminar on two-phase flow dynamics, Ohtsu, Japan, 1988
6. T. Oshinowo & M.E. Charles, *Vertical Two-Phase Flow; Part 1: Flow Pattern Correlations*, The Can. J. of Chem. Eng. vol. 52, feb. 1974, 25-35.
7. I. Žun, S. Maže & M. Livsk, *Bubble Lateral Concentration Distribution in Downward Flow*, European Two-Phase Flow Group Meeting, Rome, 1991, Conference paper F2, p. 1-17
8. N.M. Aybers & A. Tapucu, *The Motion of Gas Bubbles Rising though Stagnant Liquid*, Wärme- und Stoffübertragung, Bd. 2, (1969), 118-128
9. N.M. Aybers & A. Tapucu, *Studies on the Drag and Shape of Gas Bubbles Rising through a Stagnant Liquid*, Wärme- und Stoffübertragung, Bd. 2 (1969), 171-177
10. L.G. Leal, *Particle Motions in a Viscous Fluid*, Ann. Rev. Fluid Mech, Vol. 12 (1980) 435 476
11. T.R. Auton, *The Dynamics of Bubbles, Drops and Particles in Motion in Liquids*, Ph.D. Thesis, Univ. of

Cambridge, 1983
12. G. Hetsroni, *Handbook of Multi-Phase Systems*, McGraw-Hill Book Company, New York (NY), 1982
13. C.W.M. van der Geld & C.W.J. van Koppen, *An Overall Void Sensor and an Optical Measuring Device*, in: J.M. Delhaye & G. Cognet (editors), *Measuring Techniques in Gas-Liquid Two-Phase Flows*, Springer Verlag, Berlin, 1984, p. 525ff
14. P.C. Duineveld, *Bouncing and Coalescence of Two Bubbles in Water*, Ph.D. Thesis, Univ. of Technology Twente, 1994
15. B.P.K. Yung, H. Merry & T.R. Bott, *The Role of Turbulent Bursts in Particle Re-Entrainment in Aqueous Systems*, Chem. Eng. Sci. Vol. 44, nr. 4 (1989) 873-882
16. D. Vlaicu, C.W.M. van der Geld & B.H. Janssen, *Numerical Simulation of Turbulent Flow and Heat Transfer in a Helical Coiled Tube*, Proc. of the Seventh Workshop on Two-Phase Flow Predictions, Erlangen, 1994
17. H. Meng & C.W.M. van der Geld, *Bubble trajectories in Cross Flow and Wake Entering Mechanisms*, Proc. Int. Heat and Mass Transfer Conf, Vol. 6, pp.235-240, 214-TP-17, 1994
18. S.K. Wang, S.J. Lee. O.C. Jones Jr & R.T. Lahey Jr, *3-D Turbulence Structure and Phase Distribution Measurements in Bubbly Two-Phase Flow*, Int. J. Multiphase Flow, Vol.13, Nr. 3 (1987) 327-343
19. H.P. Riquarts, *Die Bewegungen eines Kugelförmigen Einzelkorns im Turbulenten Strömungsfeld*, Forsch. Ing.-Wes. 41 (1975) nr. 1, p.16-29
20. A.D. Gosman & E. Ioannidas, *Aspects of Computer Simulation of Liquid Fuelled Combusters*, AIAA 19th Aerospace Science Meting, paper nr. 81-0323, St. Louis, MO (1981)
21. J.O. Hinze, *Turbulence*, McGraw-Hill Book Company, New York (NY), 1975

APPENDIX

Estimate for the turbulent diffusion on bubble size

Following Riquarts [19], we assume that a bubble is moving with relative velocity v_{rel} with respect to the fluid flow with mean velocity u_f and a fluctuating component u' perpendicular to the flow direction. The fluctuating velocity is due to turbulence. The following equation is derived for the lateral displacement L_b (It is noted that in eq. (23) of Riquarts [19] an error occurs and that his particle mass density is replaced by $\frac{1}{2}\rho_f$ because of added mass):

$$L_b = \frac{\frac{2\sqrt{2}}{\pi}\sqrt{\overline{(u'_f)^2}}\,\Delta t}{1 + \frac{\pi}{18}\frac{D_b^2 \rho_f}{2\mu_f}\frac{|v_{rel}|}{L_e}}$$

Here, D_b is the bubble diameter, ρ_f is the mass density of the fluid, μ_l is the dynamic viscosity of the fluid Δt is the time of flight. Note that $L_b \sim \sqrt{\overline{(u'_f)^2}}$ if D_b is negligible small as expected.

L_e is the typical eddy length estimated by Gosman & Ioannidas [20] as:

$$L_e = c_\mu^{1/2}\frac{k^{3/2}}{\varepsilon}$$

where k is the kinetic energy of the turbulence and ε the corresponding energy dissipation rate. Coefficient c_μ is 0.09 for shear flow. The energy dissipation rate is approximated (see Hinze [21]): $\varepsilon = \rho_f c_\mu k^2/\mu_t$ where μ_t is the turbulent viscosity. In first approximation, the specific kinetic energy is given by the value for isotropic turbulence: $k = 3(u'_f)^2/2$.

To estimate the lateral bubble displacement, k is taken to be $0.1 \cdot \frac{1}{2} u_f^2$. The time of flight, Δt, is given by $3u_f$ since 3 m is the typical distance from the injection point. For u_f = 0.43 m/s and physical properties that are typical for our experiments, L_b turns out to be negligible if $D_{eq,b}$ = 6.0 mm and of the order of the tube diameter if $D_{eq,b}$ = 0.8 mm. So the lateral displacement of small-sized bubbles is enlarged by turbulent diffusion.

Table 2: Results of Migration measurements, Upflow

D_b	$V_{s,l}$	40 Ø	60 Ø	90 Ø	Rect
0.8-1.0	0.00	c 0.09	c 0.08	c 0.30 I	
	0.15			c 0.38	
	0.25	s 1.00 II	c 0.33 II		
	0.30			c 0.48	
	0.50		c 0.42		
	0.75		c 0.42		
	0.90		c 0.50		
1.2-1.7	0.00		s 0.67	s 0.80	
	0.06			s 0.60	
	0.09			w*0.30	
	0.12			w*0.30	
	0.15	II		w*0.40	
	0.20	II		w*0.30	
	0.25		II	w*0.30	
	0.30			w*0.40	
	0.35				
	0.45				(1) 0.11
	0.50		c 0.50	s 0.80	
	0.66				(1) 0.44
	0.75		c 0.50		
	0.90		s 0.58		
2.0-2.5	0.00	c 0.48		s 0.75	
	0.06			s 0.60	
	0.09			s 1.00	
	0.12			s 1.00	
	0.15	w 0.04		s 0.55	
	0.20	w 0.04		w*0.30	
	0.25	w 0.04		w*0.30 II	
	0.30	w 0.04		s 0.65	
	0.35	w 0.09			
	0.50	w 0.48			
	0.75	s 1.00			
	0.90	s 1.00			
2.9-3.7	0.45				(1) 0.25
	0.66				(1) 0.27
4.4-4.6	0.00		s 0.92		
	0.15				
	0.25		w 0.12		
	0.50		w 0.12		
	0.75		w 0.12		
	0.90		w 0.12		
5.5-6.5	0.00	w 0.25		s 0.92	
	0.15			w 0.16	
	0.25	w 0.09 III	III		
	0.30			w 0.10	
	0.50	w 0.09			
	0.75	w 0.09			
	0.90	w 0.13			
6.80	0.00	c 0.43			
⩾7.4	0.00	III s	0.92	s 0.75 III	
	0.15			s 0.58	
	0.25		s 0.67 III	III	
	0.30			s 0.58	
	0.45			s 0.58	
	0.50		s 0.83		
	0.60			s 0.67	
	0.75		s 0.67		
	0.90		s 0.75		

Table 2 continued: Downflow

D_b	$V_{s,l}$	40 Ø	60 Ø	90 Ø	Rect
1.30	0.66			s	0.50
2.00	0.45			s	0.57 III

D_b: equivalent bubble diameter [mm],
$V_{s,l}$: superficial water velocity [m/s].
*: Injected near the wall
(1): Rectangle only: centre of long wall of rectangle

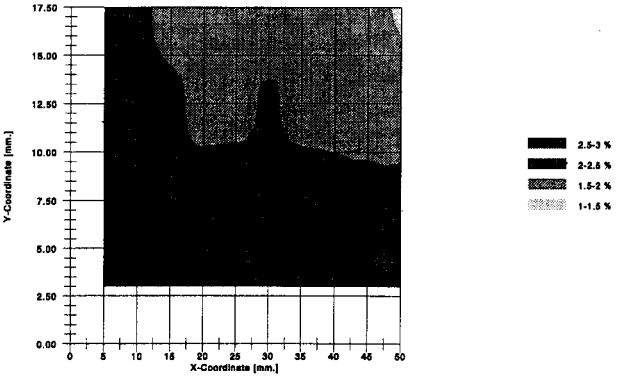

Figure 10: upflow in rectangular channel, $v_{s,l}$ = 0.45 m/s

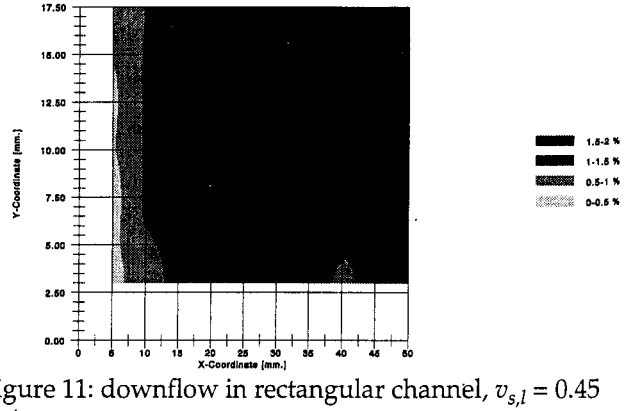

Figure 11: downflow in rectangular channel, $v_{s,l}$ = 0.45 m/s